VIP Heterogeneous Catalysis

DOI: 10.1002/anie.201209871

FePt and CoPt Nanowires as Efficient Catalysts for the Oxygen Reduction Reaction**

Shaojun Guo, Dongguo Li, Huiyuan Zhu, Sen Zhang, Nenad M. Markovic, Vojislav R. Stamenkovic, and Shouheng Sun**

The oxygen reduction reaction (ORR) is an important cathode reaction used in fuel cells and metal–air batteries for renewable energy applications.[1–3] Platinum has been studied extensively as an essential catalytic component to reduce undesired overpotentials observed in the ORR.[4] Previous computational and experimental investigations have revealed that once alloyed with first-row transition metals, such as Fe, Co, and Ni, Pt alloy thin films and nanoparticles (NPs) can show dramatic activity enhancement in ORR catalysis,[5,6] especially when the Pt-skin structure is formed on the surface of MPt.[7] This enhancement is believed to originate from the downshift of the d-band center of Pt in the alloy structure; this downshift results in a decrease of the bonding strength between Pt and the oxygenated species (often called blocking species or spectators) and an increased number of available Pt sites for oxygen adsorption.[5] Recent experiments also indicate that elongated Pt nanostructures are less subject to dissolution, Ostwald ripening, and aggregation than the Pt NPs in acidic conditions,[8–11] and that they may be robust for catalyzing the ORR with high activity and durability.

Herein, we report an advanced organic-phase synthesis of thin FePt and CoPt alloy nanowires (NWs) for enhanced catalysis of the ORR. Different from the previous approach to FePt NPs[12] and FePt NWs,[13] the current synthesis through decomposition of metal pentacarbonyl and reduction of platinum acetylacetonate, $[Pt(acac)_2]$, was performed in sodium oleate solution of 1-octadecene (ODE) and oleylamine (OAm). Depending on the metal carbonyl used, FePt or CoPt NWs were obtained at a high synthetic yield and with the desired control over alloy composition. Electrochemical studies showed that these NWs were active catalysts for the ORR. The specific activity and the mass activity of the 2.5 nm wide FePt NWs reached 1.53 mA cm^{-2} and 844 mA mg^{-1} Pt at 0.9 V (vs. reversible hydrogen electrode, RHE; 0.2 mA cm^{-2} and 110 mA mg^{-1} Pt at 0.95 V), while those of the benchmark Pt catalyst reached 0.32 mA cm^{-2} and 155 mA mg^{-1} Pt at 0.9 V (0.080 mA cm^{-2} and 35 mA mg^{-1} Pt at 0.95 V). The annealed 6.3 nm wide FePt NWs showed an even higher specific activity of 3.9 mA cm^{-2} at 0.9 V and 0.46 mA cm^{-2} at 0.95 V.

The FePt or CoPt NWs were prepared by thermal decomposition of iron pentacarbonyl, $[Fe(CO)_5]$, or dicobalt octacarbonyl, $[Co_2(CO)_8]$, and reduction of $[Pt(acac)_2]$. In the synthesis, $[Fe(CO)_5]$ or $[Co_2(CO)_8]$ was added to serve both as a reducing agent and as an Fe or Co precursor for alloying with Pt (Experimental Section). Inductively coupled plasma-atomic emission spectroscopy (ICP-AES) was used to analyze the composition of the as-prepared FePt and CoPt NWs. We found that the molar ratio of Fe/Pt or Co/Pt was important for tuning the composition of FePt or CoPt NWs. For example, the reaction of 0.5 mmol $[Pt(acac)_2]$ and 1 mmol $[Fe(CO)_5]$ led to the formation of $Fe_{68}Pt_{32}$ NWs. With a fixed amount of $[Pt(acac)_2]$ (0.5 mmol), 0.57 and 0.32 mmol of $[Fe(CO)_5]$ resulted in $Fe_{56}Pt_{44}$ and $Fe_{42}Pt_{58}$ NWs, respectively. Under the same reaction conditions with a fixed amount of $[Pt(acac)_2]$ (0.5 mmol) as in the synthesis of FePt NWs, 0.53 mmol $[Co_2(CO)_8]$ produced $Co_{63}Pt_{37}$ NWs, while 0.4 mmol $[Co_2(CO)_8]$ yielded $Co_{32}Pt_{68}$ NWs. In the synthesis of CoPt NWs, the amount of $[Co_2(CO)_8]$ added in the reaction mixture was key to the formation of NW product. Too much (270 mg, 0.795 mmol) or too little (90 mg, 0.265 mmol) $[Co_2(CO)_8]$ would result in a mixture of NPs and thick NWs (Figure S1A in the Supporting Information) or a mixture of NPs and thin NWs (Figure S1B). Figure 1 and Figure S2 in the Supporting Information show the representative transmission electron microscopy (TEM) images of the FePt and CoPt NWs with diameters at (2.5 ± 0.3) nm. The length of the FePt NWs is in the range of 30–100 nm and that of CoPt NWs in the range of 50–500 nm. The FePt and CoPt NWs were further characterized by X-ray diffraction (XRD; Figure S3 in the Supporting Information). The broadened diffraction peaks from these

[*] Dr. S. Guo,[+] D. Li,[+] H. Zhu, S. Zhang, Prof. S. Sun
Department of Chemistry, Brown University
Providence, RI 02912 (USA)
E-mail: ssun@brown.edu
D. Li,[+] Dr. N. M. Markovic, Dr. V. R. Stamenkovic
Materials Science Division, Argonne National Laboratory
Argonne, IL 60439 (USA)
E-mail: vrstamenkovic@anl.gov
[+] These authors contributed equally to this work.

[**] Supported by the U.S. Department of Energy, Office of Energy Efficiency and Renewable Energy, Fuel Cell Technologies Program.
Supporting information for this article is available on the WWW under http://dx.doi.org/10.1002/anie.201209871.

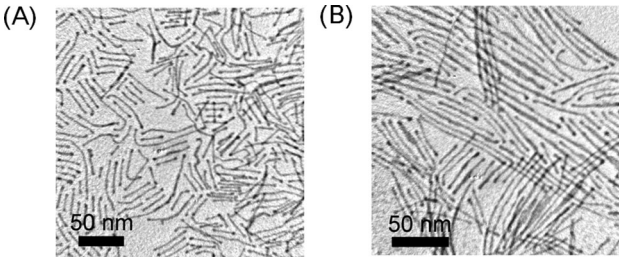

Figure 1. TEM images of A) 2.5 nm wide $Fe_{56}Pt_{44}$ and B) $Co_{63}Pt_{37}$ NWs.

NWs reveal the small dimension of the chemically disordered *fcc* crystal domains.[14]

The as-synthesized FePt and CoPt NWs were studied as catalysts in the ORR. To perform the tests, the NWs were first deposited on a carbon (C) support (Ketjen EC-300J) by sonicating the mixture of NWs and C (NW/C = 4:6 by weight) in hexane/acetone (v/v = 2:1) and then washed with acetic acid (99%) at 70°C to remove the surfactant.[15] Upon this acid wash, part of the Fe in the FePt NWs was etched away, as confirmed by the change of the composition from $Fe_{42}Pt_{58}$, $Fe_{56}Pt_{44}$, and $Fe_{68}Pt_{32}$ to $Fe_{15}Pt_{85}$, $Fe_{20}Pt_{80}$, and $Fe_{23}Pt_{77}$, respectively. After the same treatment with acetic acid, a substantial amount of Co was lost, and less than 10% Co was retained in the NW structure. This indicates that CoPt NWs are more vulnerable to acid than FePt NWs. Figure 2A shows the typical cyclic voltammograms (CVs) of the $Fe_{20}Pt_{80}$ NWs in Ar-saturated $HClO_4$ (0.1M) with a sweep rate of 50 mV s^{-1}. The corresponding CVs exhibit strong peaks associated with hydrogen adsorption/desorption below 0.4 V and Pt oxidization/reduction above 0.6 V. Figure 2B shows a typical ORR polarization curve of the $Fe_{20}Pt_{80}$ NWs obtained at room temperature in O_2-saturated $HClO_4$ (0.1M) at a sweep rate of 20 mV s^{-1} and a rotation speed of 1600 rpm. We can see that the electrochemical reduction reaches the diffusion limit below 0.8 V and a mixed kinetic-diffusion control region between 0.8 and 1.0 V. The kinetic current related to the ORR can be calculated from the polarization curve by using mass-transport correction and normalizing to electrochemically active surface area (ECASA) and Pt amount. Similarly, CoPt NWs were studied. The corresponding CVs and ORR polarization curves are shown in Figure S4 in the Supporting Information. The electrocatalytic behavior of these NWs was compared with the commercial BASF 3.2 nm Pt catalyst supported on carbon (C-Pt, 46% loading). Figure 2C shows the Tafel plots, which describe the specific activities (j_k, kinetic current density) as a function of electrode potential, and a comparison of the specific activities of $Fe_{20}Pt_{80}$ NWs, Co_8Pt_{92} NWs, and commercial Pt catalysts at 0.9 V and 0.95 V (vs. RHE) is given in Figure 2D. The specific activity of $Fe_{20}Pt_{80}$ NWs reaches 1.53 mA cm^{-2} at 0.9 V (0.20 mA cm^{-2} at 0.95 V), which is higher than that of Co_8Pt_{92} NWs (0.64 mA cm^{-2} at 0.9 V and 0.11 mA cm^{-2} at 0.95 V) and of Pt catalyst (0.32 mA cm^{-2} at 0.9 V and 0.08 mA cm^{-2} at 0.95 V). The lower activity of the Co_8Pt_{92} NWs compared to $Fe_{20}Pt_{80}$ is likely caused by the greater loss of Co from CoPt compared to that of Fe from FePt in the acid solution.

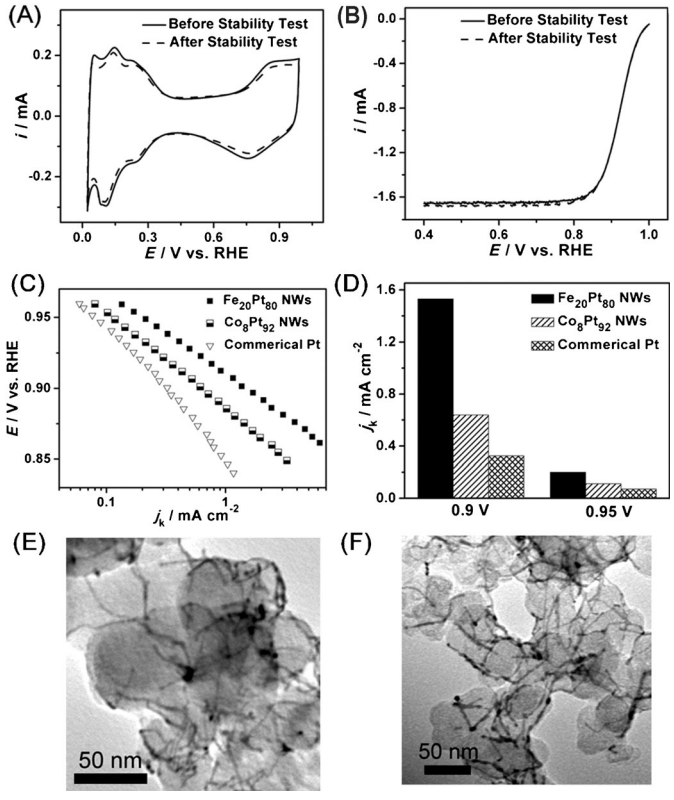

Figure 2. A) CVs and B) polarization curves of the $Fe_{20}Pt_{80}$ NWs before and after 4000 potential cycles between 0.6–1.0 V vs. RHE. C) Specific ORR activities of different catalysts with the rotating disk electrode (RDE) rotation rate at 1600 rpm (Tafel plot), and D) summary of specific ORR activities of different catalysts at 0.9 V and 0.95 V vs. RHE. E, F) TEM images of the C-$Fe_{20}Pt_{80}$ NWs before (E) and after (F) stability test. The electrocatalytic results were obtained by averaging three independent measurements with an error margin < 10%.

We further studied the stability of $Fe_{20}Pt_{80}$ NWs by scanning the potential between 0.6 and 1 V (vs. RHE) in O_2-saturated $HClO_4$ (0.1M) at a scan rate of 100 mV s^{-1}. Figure 2A,B also shows the CVs and ORR polarization curves of the $Fe_{20}Pt_{80}$ NWs after 4000 potential cycles. We can see that the $Fe_{20}Pt_{80}$ NWs lost a very small portion of their initial ECASA, and their ORR polarization curve overlaps with the one before the stability test. Once immersed into the $HClO_4$ solution, the $Fe_{20}Pt_{80}$ was changed to $Fe_{17}Pt_{83}$ and further to $Fe_{16}Pt_{84}$ after the stability test. This indicates that the Fe/Pt ratio in FePt treated with acetic acid is well stabilized and shows only a small change in the $HClO_4$ solution during the stability test. TEM analysis shows that there is no visible morphology change for $Fe_{20}Pt_{80}$ NWs (Figure 2E,F). The ORR stability performance of the Co_8Pt_{92} NWs is similar to that of the $Fe_{20}Pt_{80}$ NWs (Figure S5A,B in the Supporting Information).

We should note that the composition-dependent ORR activity of FePt and CoPt NWs is not well represented by the FePt and CoPt NWs owing to the loss of Fe and Co during the acetic acid treatment. Nonetheless, the present FePt NWs have the highest specific activity for the ORR among all reported elongated Pt-based ORR catalysts.[8,10,11] The mass activity of $Fe_{20}Pt_{80}$ NWs is 844 mA mg^{-1} Pt, exceeding the DOE 2015 target at 440 mA mg^{-1} Pt (DOE = U.S. Department of Energy).[16] The enhancement in both ORR activity and stability observed in FePt NWs arises very likely from the Pt topmost atoms arranged along a long NW facet, as well as from the strong interaction between the NWs and the carbon support, which hinders NW dissolution, Ostwald ripening, and aggregation.[8,10,11]

The thicker (6.3 nm) FePt NWs showed even better specific ORR catalysis. These NWs were synthesized by growing FePt over the preformed 2.5 nm $Fe_{56}Pt_{44}$ NWs (Experimental Section). By using this seed-mediated growth, we were able to tune the diameter of FePt NWs

from 2.5 to 6.3 nm with nearly precise composition control at $Fe_{56}Pt_{44}$. TEM images (Figure S6 in the Supporting Information) prove that these NWs are fairly uniform. XRD of these NWs (Figure S7 in the Supporting Information) shows diameter-dependent line broadening diffraction patterns, indicating that the thicker NWs have larger FePt crystal domains. These 6.3 nm FePt NWs were subject to the acid treatment and thermal annealing at 400 °C under Ar + 3 % H_2 for 2 h. The morphology of the 6.3 nm FePt NWs was nearly unchanged after these acid and annealing treatments (Figure 3 A; their composition was $Fe_{18}Pt_{82}$). In contrast, none of

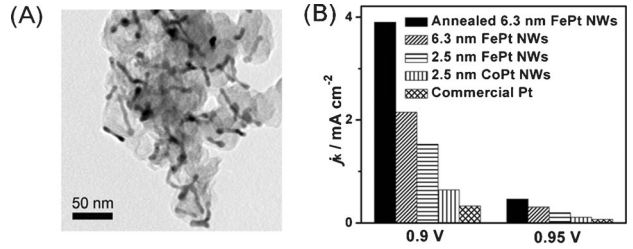

Figure 3. A) TEM image of the 6.3 nm FePt NWs deposited on the carbon support after annealed at 400 °C for 2 h in Ar + 3 % H_2. B) Summary of ORR specific activities of the annealed 6.3 nm FePt NWs, as well as of the un-annealed 6.3 nm FePt NWs, 2.5 nm FePt NWs, 2.5 nm CoPt NWs, and commercial Pt at 0.9 V and 0.95 V (vs. RHE).

the thinner NWs could survive such a combined treatment; they were broken down into irregular particulate structures (Figure S8 in the Supporting Information). A comparison of the activities of different catalysts for the ORR in $HClO_4$ (0.1 M; Figure 3 B) shows, that the treated 6.3 nm FePt NWs have the best ORR specific activity at 3.9 mA cm^{-2} at 0.9 V (vs. RHE) and 0.46 mA cm^{-2} at 0.95 V. The ORR stability of the 6.3 nm FePt NWs was also studied in O_2-saturated $HClO_4$ (0.1 M) by cycling the potentials between 0.6–1.0 V (vs. RHE) for 4000 cycles. As shown in the CVs (Figure S9A in the Supporting Information) and ORR polarization curves (Figure S9B), the treated 6.3 nm FePt NWs have no ECASA drop and ORR polarization shift.

The enhanced ORR activity and stability of the acid/annealing-treated 6.3 nm FePt NWs is likely caused by the formation of Pt skin on the surface of NWs, similar to what has been demonstrated in the MPt alloy NPs.[7,17–19] The formation of Pt skin along each 6.3 nm FePt NW may be proved by CVs (Figure S9C) and CO stripping curves (Figure S9D) of the annealed 6.3 nm FePt NWs, which show the typical suppressed H_{upd} region (H_{upd} = underpotentially deposited hydrogen; Figure S9C) and the intensity drop of the CO oxidation peak (Figure S9D) associated with the presence of a Pt-skin surface.[17–19] Owing to the altered electronic/adsorption properties of a Pt-skin surface, the CO stripping peak was used to estimate the ECASA of the catalyst by integrating the area of the CO stripping peak.[19] The ECASA of the annealed 6.3 nm FePt NWs was estimated to be 1.51 cm^2, which was larger than 1.22 cm^2 determined from the conventional approach using the H_{upd} curve. This is characteristic of the formation of a Pt-skin structure.[17,19] We should note that under the same testing conditions, the mass activity of the acid-treated 6.3 nm FePt NWs is lower than that of the 2.5 nm FePt NWs owing to the larger percentage of Pt embedded inside the 6.3 nm FePt NWs.

In summary, FePt (or CoPt) NWs have been synthesized in high yield by using a simple organic-phase decomposition of $[Fe(CO)_5]$ (or $[Co_2(CO)_8]$) and reduction of $[Pt(acac)_2]$ in a solution of ODE and OAm containing sodium oleate. By controlling the molar ratio of $[Fe(CO)_5]$ or $[Co_2(CO)_8]$ to $[Pt(acac)_2]$, the FePt (or CoPt) NW composition can be readily tuned. When treated with acetic acid, these FePt (or CoPt) NWs become active and stable for the catalysis of the ORR. The surface specific and mass activities of the FePt NWs reach 1.53 mA cm^{-2} and 844 mA mg^{-1} Pt, which are 4.7 and 5.5 times higher than those of the commercial BASF 3.2 nm Pt catalyst. The FePt or CoPt NWs are also very stable in $HClO_4$ (0.1 M) solution with almost no ECASA drop and ORR polarization shift after the stability test. The annealed 6.3 nm FePt NWs showed an even higher specific activity of 3.9 mA cm^{-2}. These NWs represent a new class of robust catalysts for the ORR and may be more applicable in practical fuel cells and other related energy devices.

Experimental Section

Synthesis of 2.5 nm MPt (M = Fe, Co) NWs: Under a gentle nitrogen flow and magnetic stirring, sodium oleate (0.3 g) was dissolved in ODE (12 mL) by heating the suspension to 180 °C. The solution was cooled to 60 °C, followed by the addition of $[Pt(acac)_2]$ (0.2 g) and OAm (8 mL) and further heating to 115 °C. Under a blanket of nitrogen, different amounts of $[Fe(CO)_5]$ and $[Co_2(CO)_8]$ (dissolved in 1,2-dichlorobenzene) were injected into the reaction solution. The solution was further heated to 240 °C at a heating rate of 4–5 °C min^{-1} and kept at this temperature for 25 min to make FePt and CoPt NWs with different compositions. Hexane (30 mL) and ethanol (50 mL) were added to precipitate the product. The product was separated by centrifugation at 9500 rpm for 10 min.

Seed-mediated synthesis of FePt NWs thicker than 2.5 nm: $[Pt(acac)_2]$ (0.08 g) was dissolved in ODE (10 mL), OAm (1 mL), and OA (1 mL) by heating the mixture to 115 °C under N_2 protection. $Fe_{56}Pt_{44}$ NWs (30 mg) dispersed in ODE (2 mL) and $[Fe(CO)_5]$ (0.032 mL) were added under a N_2 blanket. The solution was then heated to 240 °C and kept at this temperature for 25 min. The solution was cooled to room temperature, and ethanol (25 mL) was added to precipitate the NWs by centrifugation (8500 rpm, 8 min). The product (3.7 nm FePt NWs) was dispersed in hexane (25 mL) and precipitated by adding ethanol (25 mL). It was redispersed in hexane (10 mL) for either catalytic use or for further NW growth. Under the same conditions as in the synthesis of 3.7 nm FePt NWs, 40 mg $[Pt(acac)_2]$ and 0.016 mL $[Fe(CO)_5]$ led to 4.6 nm FePt NWs, whereas 60 mg $[Pt(acac)_2]$/0.024 mL $[Fe(CO)_5]$ and 80 mg $[Pt(acac)_2]$/0.032 mL $[Fe(CO)_5]$ yielded 5.5 and 6.3 nm FePt NWs, respectively.

NW activation for the ORR: NWs (20 mg in 20 mL hexane) were mixed with Ketjen carbon (30 mg) suspended in a mixture of hexane/acetone (v/v 2:1, 30 mL). The mixture was sonicated for 1 h. The loading amounts of NWs on the carbon support were calculated to be 25.2 % and 23.8 % for FePt and CoPt, respectively, according to the ICP results. The C-NW catalyst was separated by centrifugation, washed two times with hexane, and mixed with acetic acid (30 mL). The suspension was heated at 70 °C for overnight.[15] Thermal annealing of the C-FePt NWs was performed under a condition similar to the treatment of C-NiPt NPs.[17,18] The as-prepared C-FePt NWs were first thermally treated in air at 200 °C overnight, and then mixed with $HClO_4$ (0.1 M, 20 mL) overnight to remove Fe on the

surface of FePt NWs. Finally, the acid-treated C-FePt NWs were annealed in Ar + 3% H_2 at 400 °C for 2 h. All catalysts were dispersed in a mixture containing water, isopropanol, and Nafion (5%) (v/v/v 4:1:0.05) to form a 2 mg mL^{-1} ink.

Electrochemical test: 20 μL of catalyst ink (2 mg mL^{-1}) were casted on the newly polished glassy carbon electrode and dried at ambient condition. The Pt loading amount was 6.50 and 4.52 μg for FePt and CoPt, respectively. The test solution was $HClO_4$ (0.1 M). The catalysts were cycled at room temperature with a scanning rate of 50 mV s^{-1} in the Ar-saturated solution until stable CVs were obtained. The ORR polarization curves were measured at a scanning rate of 10 or 20 mV s^{-1} in the O_2-saturated $HClO_4$ (0.1 M) solution at 1600 rpm.

Received: December 10, 2012
Published online: February 18, 2013

Keywords: alloys · heterogeneous catalysis · nanostructures · oxygen reduction reaction · platinum

[1] a) Y. Liang, Y. Li, H. Wang, J. Zhou, J. Wang, T. Regier, H. Dai, *Nat. Mater.* **2011**, *10*, 780 – 786; b) C.-H. Cui, H.-H. Li, J.-W. Yu, M.-R. Gao, S.-H. Yu, *Angew. Chem.* **2010**, *122*, 9335 – 9338; *Angew. Chem. Int. Ed.* **2010**, *49*, 9149 – 9152.

[2] J. Suntivich, H. A. Gasteiger, N. Yabuuchi, H. Nakanishi, J. B. Goodenough, S.-H. Yang, *Nat. Chem.* **2011**, *3*, 546 – 550.

[3] Y.-C. Lu, Z. Xu, H. A. Gasteiger, S. Chen, K. Hamad-Schifferli, S.-H. Yang, *J. Am. Chem. Soc.* **2010**, *132*, 12170 – 12171.

[4] Y.-J. Wang, D. P. Wilkinson, J. Zhang, *Chem. Rev.* **2011**, *111*, 7625 – 7651.

[5] a) V. R. Stamenkovic, B. Mun, S. M. Arenz, K. J. J. Mayrhofer, C. A. Lucas, G. Wang, P. N. Ross, N. M. Markovic, *Nat. Mater.* **2007**, *6*, 241; b) V. R. Stamenkovic, B. Fowler, B. S. Mun, G. F. Wang, P. N. Ross, C. A. Lucas, N. M. Markovic, *Science* **2007**, *315*, 493 – 497.

[6] See examples: a) J. Wu, J. Zhang, Z. Peng, S. Yang, F. T. Wagner, H. Yang, *J. Am. Chem. Soc.* **2010**, *132*, 4984 – 4985; b) J. Wu, L. Qi, H. You, A. M. Gross, J. Li, H. Yang, *J. Am. Chem. Soc.* **2012**, *134*, 11880 – 11883; c) J. Kim, Y. Lee, S. Sun, *J. Am. Chem. Soc.* **2010**, *132*, 4996 – 4997; d) J. Wu, A. Gross, H. Yang, *Nano Lett.* **2011**, *11*, 798 – 802.

[7] a) C. Wang, M. Chi, D. Li, D. Strmcnik, D. van der Vliet, G. Wang, V. Komanicky, K.-C. Chang, A. P. Paulikas, D. Tripkovic, J. Pearson, K. L. More, N. M. Markovic, V. R. Stamenkovic, *J. Am. Chem. Soc.* **2011**, *133*, 14396 – 14403; b) L. Gan, M. Heggen, S. Rudi, P. Strasser, *Nano Lett.* **2012**, *12*, 5423 – 5430.

[8] S. Sun, G. Zhang, D. Geng, Y. Chen, R. Li, M. Cai, X. Sun, *Angew. Chem.* **2011**, *123*, 442 – 446; *Angew. Chem. Int. Ed.* **2011**, *50*, 422 – 426.

[9] a) C. Koenigsmann, W.-P. Zhou, R. R. Adzic, E. Sutter, S. S. Wong, *Nano Lett.* **2010**, *10*, 2806 – 2811; b) B. Y. Xia, W. T. Ng, H. B. Wu, X. Wang, X. W. Lou, *Angew. Chem.* **2012**, *124*, 7325 – 7328; *Angew. Chem. Int. Ed.* **2012**, *51*, 7213 – 7216.

[10] Z. Chen, M. Waje, W. Li, Y. Yan, *Angew. Chem.* **2007**, *119*, 4138 – 4141; *Angew. Chem. Int. Ed.* **2007**, *46*, 4060 – 4063.

[11] C. Koenigsmann, A. C. Santulli, K. Gong, M. B. Vukmirovic, W.-P. Zhou, E. Sutter, S. S. Wong, R. R. Adzic, *J. Am. Chem. Soc.* **2011**, *133*, 9783 – 9795.

[12] a) S. Sun, C. B. Murray, D. Weller, L. Folks, A. Moser, *Science* **2000**, *287*, 1989 – 1992; b) S. H. Sun, *Adv. Mater.* **2006**, *18*, 393 – 403.

[13] C. Wang, Y. Hou, J. Kim, S. Sun, *Angew. Chem.* **2007**, *119*, 6449 – 6451; *Angew. Chem. Int. Ed.* **2007**, *46*, 6333 – 6335.

[14] S. Guo, S. Zhang, X. Sun, S. Sun, *J. Am. Chem. Soc.* **2011**, *133*, 15354 – 15357.

[15] a) V. Mazumder, S. Sun, *J. Am. Chem. Soc.* **2009**, *131*, 4588 – 4589; b) S. Guo, S. Sun, *J. Am. Chem. Soc.* **2012**, *134*, 2492 – 2495.

[16] U.S. Department of Energy, Technical Plan: Fuel Cells, **2007** (http://www1.eere.energy.gov/hydrogenandfuelcells/mypp/pdfs/fuel_cells.pdf).

[17] a) C. Wang, D. Li, M. Chi, J. Pearson, R. B. Rankin, J. Greeley, Z. Duan, G. Wang, D. van der Vliet, K. L. More, N. M. Markovic, V. R. Stamenkovic, *J. Phys. Chem. Lett.* **2012**, *3*, 1668 – 1673; b) J. Hou, Y. Shao, M. W. Ellis, R. B. Moored, B. Yi, *Phys. Chem. Chem. Phys.* **2011**, *13*, 15384 – 15402.

[18] D. F. van der Vliet, C. Wang, D. Tripkovic, D. Strmcnik, X. F. Zhang, M. K. Debe, R. T. Atanasoski, N. M. Markovic, V. R. Stamenkovic, *Nat. Mater.* **2012**, *11*, 1051 – 1058.

[19] D. F. van der Vliet, C. Wang, D. Li, A. P. Paulikas, J. Greeley, R. B. Rankin, D. Strmcnik, D. Tripkovic, N. M. Markovic, V. R. Stamenkovic, *Angew. Chem.* **2012**, *124*, 3193 – 3196; *Angew. Chem. Int. Ed.* **2012**, *51*, 3139 – 3142.

